Published in final edited form as:
Cell Transplant. 2013 ; 22(2): 231–242. doi:10.3727/096368912X654939.

Human-Scale Whole-Organ Bioengineering for Liver Transplantation: A Regenerative Medicine Approach

Hiroshi Yagi[*], **Ken Fukumitsu**[†], **Kazumasa Fukuda**[*], **Minoru Kitago**[*], **Masahiro Shinoda**[*], **Hideaki Obara**[*], **Osamu Itano**[*], **Shigeyuki Kawachi**[*], **Minoru Tanabe**[*], **Gina M. Coudriet**[‡], **Jon D. Piganelli**[‡], **Thomas W. Gilbert**[§], **Alejandro Soto-Gutierrez**[†,§], and **Yuko Kitagawa**[*]

[*]Department of Surgery, School of Medicine, Keio University, Shinjuku-ku, Tokyo, Japan

[†]Department of Pathology, Center for Innovative Regenerative Therapies, Department of Surgery, Transplantation Section, Children's Hospital of Pittsburgh and the Starzl Transplantation Institute, University of Pittsburgh, Pittsburgh, PA, USA

[‡]Department of Pediatrics, Division of Immunogenetics/Immunology, Children's Hospital of Pittsburgh of UPMC, Pittsburgh, PA, USA

[§]McGowan Institute for Regenerative Medicine, Departments of Surgery, Cardiothoracic Surgery, and Bioengineering, University of Pittsburgh, Pittsburgh, PA, USA

Abstract

At this time, the only definitive treatment of hepatic failure is liver transplantation. However, transplantation has been limited by the severely limited supply of human donor livers. Alternatively, a regenerative medicine approach has been recently proposed in rodents that describe the production of three-dimensional whole-organ scaffolds for assembly of engineered complete organs. In the present study, we describe the decellularization of porcine livers to generate liver constructs at a scale that can be clinically relevant. Adult ischemic porcine livers were successfully decellularized using a customized perfusion protocol, the decellularization process preserved the ultrastructural extracellular matrix components, functional characteristics of the native microvascular and the bile drainage network of the liver, and growth factors necessary for angiogenesis and liver regeneration. Furthermore, isolated hepatocytes engrafted and reorganized in the porcine decellularized livers using a human-sized organ culture system. These results provide proof-of-principle for the generation of a human-sized, three-dimensional organ scaffold as a potential structure for human liver grafts reconstruction for transplantation to treat liver disease.

Keywords

Whole-organ scaffold; Liver tissue engineering; Decellularization; Bile duct; Porcine liver; Regenerative medicine; Bioengineering in organ transplantation

Address correspondence to Alejandro Soto-Gutierrez, M.D., Ph.D., Department of Pathology and Surgery, Transplantation Section, Children's Hospital of Pittsburgh, University of Pittsburgh, 3511 Rangos Research Building 530 45th Street, Pittsburgh, PA 15201, USA. Tel: +1 (412) 692-5562; Fax: +1 (412) 692-6599; sotogutierreza@upmc.edu or Yuko Kitagawa, M.D., Ph.D., FACS, Department of Surgery, School of Medicine, Keio University, 35 Shinanomachi, Shinjuku-ku, Tokyo 160-8582, Japan. Tel: +(81)-3-3353-1211 ext. 62334; Fax: +(81)-3-3355-4707; kitagawa@a3.keio.jp.

The authors declare no conflicts of interest.

INTRODUCTION

It is considered that about 27,000 deaths are registered annually in the United States due to liver disease (13). To date the only definitive treatment for end-stage liver failure is orthotopic transplantation. And it is estimated that the high prevalence of hepatitis C will increase the demand significantly in the next decade (7). Conversely, the donor pool is expected to shrink since obesity rates continue to increase, as steatosis is a significant risk factor in liver transplantation (2). Several approaches (e.g., xenotransplantation) have been proposed to increase the number of potential donor organs. However, previous attempts in humans often resulted in hyperacute rejection and death (22). A much more elegant solution to liver disease is hepatocyte transplantation, and laboratory studies and experiences in small numbers of human subjects have demonstrated its efficacy. Unfortunately, cell transplantation therapy is also limited by the severe shortage of donor cells as well as by low engraftment efficiency. Nevertheless, new strategies to enhance cell engraftment and repopulation suggest the benefits of radiation therapy with potential clinical translation in the near future (31).

Recently, interest in decellularization techniques has increased significantly, wherein removal of the cells from an organ leaves a complex mixture of structural and functional proteins that constitute the extracellular matrix (ECM) (6,27). There is significant evidence indicating that local environment factors induce hepatocytes homing, differentiation, and proliferation (14,16,26). Moreover, an increasingly large body of literature indicates that tissue-specific gene expression, morphogenesis, and cell migration are promoted by interactions between cells and the surrounding ECM and liver is not an exception (11,23). Thus, it is reasonable that the three-dimensional native liver ECM would support the viability, phenotype, function, and tissue assembly of hepatocytes.

Recent studies have shown that decellularization of whole organs such as livers (4,5,28,29), lung (19,21), and heart (20) are possible in rodent models. However, the development of human size whole-organ decellularization to engineer liver grafts for transplantation is necessary. The number of available discarded livers that could be used for decellularization/recellularization processes are estimated in the order of hundreds (13). Therefore, the concept of engineering liver grafts from discarded organ ECM is feasible without affecting the number of organs that actually are reserved for transplantation.

The objectives of the present study were to establish an effective and minimally disruptive method for the decellularization of intact porcine whole liver and to demonstrate that reseeding of hepatocytes is possible, resulting in the construction of three-dimensional scaffold material with liver parenchymal cells. The methods and techniques established in this study represent a significant step towards the decellularization and recellularization procedures necessary for a successful regenerative medicine approach to liver bioengineering for transplantation at a human scale.

MATERIALS AND METHODS

Animals

All experimental procedures and protocols were approved by the Animal Ethics Committee of the Keio University, School of Medicine. The animals were treated according to the guidelines of the Ministry of Education, Culture, Sports, Science and Technology, Japan.

Male LWD porcine weighing 20–23 kg (Central Research Institute for Feed and Livestock, Ibaraki, Japan) were used for liver harvest for decellularization ($n = 8$) or hepatocyte isolation ($n = 7$). Animals were anesthetized by midazolam 0.2 mg/kg (Astellas, Tokyo,

Japan) and medetomidine 0.08 mg/kg (Zenoaq, Fukushima, Japan), followed by isofluorane inhalation to keep anesthesia during the procedure connected to a standard respiratory system, consisting of an endotracheal tube for continuing inhalation. The surgical procedures were performed in the fully equipped animal research laboratory located in the Laboratory Animal Center.

Surgical Procedure

Using a vertical midline incision, the porcine underwent laparotomy and the gallbladder was removed. The infrahepatic vena cava (IVC) was isolated from the inferior margin of the liver to the level of the renal veins. The liver was then retracted ventrally and superiorly, and the posterior diaphragmatic attachments of the liver were divided. The hepatoduodenal ligament was opened, the common bile duct was isolated, and Safeed Tube 2.7 mm (8 Fr) (Terumo, Tokyo, Japan) was inserted when corrosion casting or cholangiography was performed. Next after the splenic artery and the left gastric artery are ligated and divided, the celiac artery and the portal vein were isolated. After an intravenous injection of heparin (100 U/kg), Safeed Tube 2.7 mm (8 Fr) and 6 mm (18 Fr) (Terumo, Tokyo, Japan) were inserted via the celiac artery and the portal vein, respectively. Heparinized 0.9% saline (1,500 ml) was infused from the portal vein, while IVC and supra hepatic vena cava (SHVC) was transected. After the saline infusion, the liver was removed and weighed. It was freshly used for hepatocyte isolation and preserved at 4°C or frozen at −80°C for a minimum of 12 h prior to decellularization.

Whole-Organ Liver Decellularization

The frozen livers were thawed at 4°C and subsequently washed with PBS overnight to remove blood through perfusion via portal vein at 30 ml/min. Decellularization was achieved by perfusing the liver with sodium dodecyl sulfate (SDS; Sigma, St. Louis, MO, USA) in deionized water for a total of 72–96 h starting with 0.01% SDS for 24 h followed by 0.1% SDS for another 24 h, which was followed by 1% SDS for 48 h or more. Subsequently, the liver was washed with deionized water 15 min and with 1% Triton X-100 (Sigma) for 30 min. The decellularized livers were washed with PBS for 1 h. The liver bioscaffold was sterilized in 0.1% peracetic acid (Sigma) in PBS for 3 h. The liver bioscaffold was washed extensively with sterile PBS and preserved in PBS supplemented with antibiotics and kept at 4°C for up to 7 days.

Hepatocyte Isolation and Culture

The whole liver weight was 506 ± 27.6 g ($n = 5$). The right lateral lobes, weighing 127 ± 11 g, were surgically removed for hepatocyte isolation. Hepatocytes were isolated with a four-step retrograde dispase/collagenase perfusion method as previously described (15). After isolation, the cells were suspended with Dulbecco's modified Eagle's medium (DMEM; Sigma-Aldrich, St. Louis, MO, USA), and the cell viability was determined by try-pan blue exclusion test (Sigma-Aldrich). Cell yield was $1.4 \times 10^9 \pm 0.2$ per isolation ($n = 7$), which is about 11×10^6 cells/g of liver weight, and the viability was 91.8 ± 2.4% (assessed by trypan blue). Cells (0.25×10^6) in each well were cultured on a single collagen layer with rat type 1 collagen (BD Biosciences, Bedford, MA, USA) of 24-well plates up to 7 days as a control. For 3D hepatocyte culture control, 0.25×10^6 hepatocytes were plated onto 24-well tissue culture dishes precoated with collagen type I (BD Biosciences), according to the methods of Dunn et al. (9). After cell attachment, monolayers were overlaid with ice-cold medium containing 0.25 mg/ml Matrigel (BD Biosciences) as described elsewhere for collagen-Matrigel sandwich culture (17). Additional 500 μl of culture medium was supplied and cells were incubated up to 7 days at 37°C and 5% CO_2. Medium was changed every day.

Vascular Corrosion Casting

Corrosion casts were prepared using Batson's 17 anatomic corrosion kit following manufacturer's recommendations (Polysciences, Inc., Warrington, PA, USA). Polymer mixture (20–40 ml), depending on the liver size, was injected via inserted tubes of the infrahepatic vena cava, portal vein, hepatic artery, or biliary tree. Polymerization took at least 12 h at 4°C and was followed by maceration in 1N KOH solution for 5–12 h at 50°C.

DNA Quantification

The decellularized liver matrix was cut into small pieces and placed in centrifuge tubes. Five samples were taken from each lobe; right lateral, right median, left median, and left lateral lobe. Specifically, each lobe was dissected into two pieces vertically along the main portal vein, and the samples were taken one from the edge, one from the surface, two from the center of the lobe close to the portal vein, and one from the proximal edge close to the porta hepatis. DNA content in the liver matrix was determined according to Gilbert et al. (10) and as previously reported (28). The molecular weight of the extracted DNA was quantified using 2% agarose gel electrophoresis using 1-kb DNA ladder (Invitrogen, Tokyo, Japan) with a DNA sample extracted from normal porcine liver as a control.

Albumin Enzyme-Linked Immunosorbent Assay and Urea Assay

Albumin concentrations were determined by a competitive enzyme-linked immunosorbent assay (ELISA) using pig albumin ELISA kit (Bethyl Laboratories, Inc., Montgomery, TX, USA) following manufacturer's instruction. Urea concentration was measured using QuantiChrom™ urea assay kit (Bioassay Systems, Hayward, CA, USA). The absorbance was measured in Sunrise™ microplate reader (TECAN, Mannedorf, Switzerland). The values were normalized by cell number.

Histological Analyses

Normal fresh liver, decellularized liver matrix and recellularized liver sample at days 1, 4, and 7 were fixed with 10% formalin, embedded in paraffin, and processed for hematoxylin and eosin staining or Heidenhain's AZAN trichrome stain as well as terminal deoxynucleotidyl transferase dUTP nick end labeling (TUNEL) stain according to the manufacturer's instruction (Promega, Fitchburg, WI, USA). Additional samples were permeabilized and incubated with rabbit polyclonal anti-collagen IV, rabbit polyclonal anti-fibronectin, and rabbit polyclonal anti-laminin (Abcam, Cambridge, MA, USA) or rabbit polyclonal anti-hepatocyte growth factor (HGF; Santa Cruz Biotechnology, Inc., Santa Cruz, CA, USA), rabbit polyclonal anti-basic fibroblast growth factor (bFGF; Advanced Targeting Systems, San Diego, CA, USA), mouse monoclonal anti-vascular endothelial growth factor (VEGF; Novus Biologicals, Littleton, CO, USA), goat polyclonal anti-insulin-like growth factor (IGF-1; Abcam), and goat polyclonal anti-albumin (ALB; Bethyl Laboratories, Inc.). Secondary antibodies were goat anti-rabbit IgG and goat anti-mouse IgG and donkey anti-goat IgG (Life Technologies, Grand Island, NY, USA), and counter staining was performed with DAPI (Life Technologies). Quantification of positive areas was performed in 10 random 20× images per sample using the public software ImageJ.

Scanning Electron Microscopy

Decellularized liver samples were fixed in 2.5% glutaraldehyde in 0.2 M sodium phosphate buffer (Sigma-Aldrich) for 24 h at room temperature. The fixed samples were washed three times with fresh buffer. The samples were dehydrated with a series of ethanol solutions of increasing concentration, 70%, 80%, 90%, and 100%. The samples were dried in a Critical Point Dryer (Tousimis, Rockville, MD, USA) and sputter coated with chromium. The samples were visualized using S4000 field emission scanning electron microscope (Hitachi,

Tokyo, Japan). Normal fresh porcine liver was used as control. Disruption of the Glisson's capsule was counted if the diameter was more than 5 μm. Quantification was performed in at least 10 random places on each sample.

Digital Radiographic Evaluation of the Biliary Tree

Sodium Iotalamate (Conray, Daiichi Sankyo, Tokyo, Japan) was injected through an inserted Safeed tube into common bile duct of normal or decellularized porcine liver, and the continuous cholangiography was taken using digital cinema mode of the mobile C-arm imaging system (Arcadis Avantic, Siemens, Berlin, Germany) at 52 kV/0.3 mA.

Recellularized Liver Graft Perfusion System

Prior to the perfusion culture experiments, we performed ultraviolet irradiation to the liver scaffold for 1 h for decontamination, and the decellularized liver was transferred to a customized organ culture chamber, which was specifically constructed for a large-scale organ perfusion; the perfusion system was designed based on previously developed system for rat liver (29) that consisted of a peristaltic pump, bubble trap, and oxygenator. The system was placed in an incubator for temperature control, and the oxygenator was connected to atmospheric gas mixture. The graft was continuously perfused through the portal vein at 4 ml/min with continuous oxygenation that delivered an inflow partial oxygen tension of ~300 mmHg. The medium was changed daily. The perfusate consisted of basal medium (DMEM), 20 ng/L epidermal growth factor (EGF; Invitrogen, Carlsbad, CA, USA), 7.5 μg hydrocortisone, 1 ml/L insulin, 14.3 ng/ml glucagon (Sigma-Aldrich), 100 U/ml penicillin, and 100 mg/L streptomycin (Invitrogen, Carlsbad, CA, USA). The cells were seeded by intra-portal multistep infusion method, which was previously reported (28); a total of 1×10^9 cells (hepatocytes) were infused into the circuit in multisteps at 5–10 min intervals through a port located in the perfusion system just before the location of the perfused decellularized liver matrix ($n = 4$ for histological evaluations and $n = 3$ for functional analysis). To calculate the engraftment efficiency, the perfusate was collected, and the number and viability of cells not retained in the liver was determined with a hemacytometer and trypan blue exclusion. The total number of cells retained in the decellularized liver represented the difference between the initial number of cells seeded and the number of cells present in the perfusate after seeding.

Statistical Analysis

The mean values for the DNA content of each liver lobe were compared by one-way analysis of variance (ANOVA) followed by Scheffe's method, and the mean values for protein synthesis in each time point was compared by one-way analysis of variance (ANOVA) followed by Fisher PLSD respectively performed with IBM-SPSS statistics version 19 for Macintosh (SPSS, Chicago, IL, USA) and the number of defects on a capsule, which were more than 5 μm in width, observed on the surface of normal porcine liver and decellularized porcine liver were compared by Student's *t* test performed with Prism (GraphPad Software, La Jolla, CA, USA). A value of $p < 0.05$ was considered significant.

RESULTS

Whole-Organ Porcine Liver Homogeneous Decellularization

To determine if the decellularization protocol was feasible in large livers, we used native whole porcine livers, which are similar to human in size and anatomy. The decellularization protocol consisted first of a freezing–thawing technique for at least 12 h to induce cellular lysis. The whole organ decellularization was achieved then by portal perfusion with SDS, which is an anionic detergent that simultaneously can lyse cells and solubilize cytoplasmic

components. The protocol was based on the rat liver decellularization protocol that we previously developed (29) and is founded on the work published by Ott et al. (20). Figure 1a–e shows macroscopic images of liver prior to decellularization and after various steps in the decellularization process. This protocol could create an acellular scaffold of porcine liver, which retained the gross shape of the whole organ.

DNA Content Analysis of the Decellularized Porcine Liver Matrix

Immunological reaction of the remaining materials of the decellularized liver matrix has to be avoided if further clinical application is intended in order to elude any inflammatory reactions (10). As porcine livers have a much larger tissue density and area, we analyzed the DNA content of the different areas and lobes in order to measure the homogeneity of the decellularization process. Samples involved the right lateral, right median, left median, and left lateral lobe of the decellularized whole liver (Fig. 1f). DNA content was decreased from 98.8 ± 0.8% in all the liver lobes; 0.06 ± 0.01 μg/mg dry weight (right lateral), 0.04 ± 0.01 μg/mg dry weight (right median), 0.2 ± 0.03 μg/mg dry weight (left median), and 0.18 ± 0.04 μg/mg dry weight (left lateral), when compared to normal liver (12.12 ± 0.8 μg/mg dry weight) (Fig. 1g), indicating significant reduction of nuclear material of the whole liver.

Extracted DNA was quantified by agarose gel electrophoresis, which showed smearing of the fragmented DNA bands from decellularized liver samples (Fig. 1h). Histological analysis with H&E stain (Fig. 1i) and with DAPI (Fig. 1j) showed no visible nuclear material in the decellularized liver matrix.

Vascular and Bile Duct Morphology

It is essential to maintain a three-dimensional structure of the engineering bioscaffold to generate further transplantable liver grafts, especially the vascular network and bile duct tree are important features for subsequent recellularization and surgical implantation.

The intricate vascular network (portal veins, hepatic arteries, and hepatic veins) remains intact as assessed by the corrosion cast of the liver bioscaffold similar to normal porcine liver (Fig. 2a, b). Demonstrating clearly that those vessels retained their luminal diameter and shape. In addition, bile duct structures were mostly intact; however, we observed minimal disruption of the smaller branches (Fig. 2b). We performed digital radiographic evaluation of the biliary tree demonstrating that the larger bile ducts were well enhanced by the infusion of the contrast agent as if they had a natural structure; however, the localized retentions of the contrast agent were observed in the peripheral ends of the biliary tree of decellularized livers, while no retentions were seen in those of normal porcine liver (Fig. 2c). To evaluate the integrity of the microvasculature and surface capsule integrity, heparinized blood perfusion via portal vein was perfused and demonstrated that a vascular network retained intact inside of the livers and the flow moved through structures consistent with the hepatic veins; moreover, no leakage was determined from the liver surface, in opposition to what has been observed in rat livers (Fig. 2d, e).

Morphology

Histological analysis of the decellularized liver, especially Azan staining, revealed that collagen fibers were well retained in the decellularized scaffold showing the small lobular components in detail (Fig. 3a). In addition, immunolabeling characterization of the liver ECM showed the preservation of collagen type IV, fibronectin, and laminin, indicating a similar structural composition of the matrix to that of intact porcine liver (Fig. 3b). Ultrastructural characterization of the decellularized liver matrix was performed using scanning electron microscopy (SEM) images comparing to porcine normal liver (Fig. 3c) and confirmed the presence of structures resembling the hepatic lobules (Fig. 3d), the portal

triad (Fig. 3d), the central veins (Fig. 3e), large portal veins (Fig. 3f), and the microporous structure of the parenchyma (Fig. 3d). To generate transplantable liver scaffold, it is critical to keep the integrity of the surface (i.e., Glisson's capsule) to avoid leakage of the blood flow in case of vascularization of the liver graft. We evaluated impairments of the surface on the decellularized structure meticulously and found that most of the liver surface area was intact (1.1 ± 1/field) similar to that observed in normal porcine livers (0.4 ± 1/field) (Fig. 3e–g).

Growth Factors Content

To determine if the decellularized native liver derived bioscaffold could provide a suitable environment for cells by providing not only a three-dimensional structure but also maintaining bioactive molecules, we evaluated the expression of the growth factors such as HGF, bFGF, VEGF, and IGF-1 in the scaffold. Those factors are essential for liver regeneration and angiogenesis. While HGF and bFGF was highly expressed on the cells in the parenchyma and on the cells in the vessel walls, respectively, in normal liver, there was a lower expression in the scaffold even after the decellularization. The positive area for HGF and bFGF per field was 3.7 ± 3.6/field and 5.6 ± 4/field, respectively, compared to the normal liver (HGF: 19.7 ± 13/field, bFGF: 27.4 ± 10/field) (Fig. 4a, b). Interestingly, VEGF, which is mainly released from endothelial cells as one of the critical growth factor for angiogenesis, was also observed in the acellular matrix (4.3 ± 2.9/field), and the normal liver was (22.4 ± 8.6/field) (Fig. 4c). In addition, IGF-1, which is released from hepatocyte, was also observed in acellular scaffold. The expression in acellular scaffold (1.8 ± 1.2/field) was relatively lower than that of normal liver (14.7 ± 8.3/field) (Fig. 4d). These results indicated that at least epitopes of each growth factors, approximately 19% of HGF, 20% of bFGF, 19% of VEGF, and 13% of IGF-1, were preserved in the decellularized liver matrix when compared with native liver.

Recellularization

To determine if porcine primary hepatocytes could efficiently be delivered in this large-scale liver bioscaffold, an organ chamber was manufactured that contains a sterile main reservoir in which the decellularized liver matrix is mounted (Fig. 5a), we selected the multistep infusion protocol based in our previous work in rodents (28,29). Isolated porcine hepatocytes (1×10^9) with 91.8 ± 2.4% viability ($n = 7$) were infused through the portal vein using the large-scale perfusion chamber (Fig. 5a). Twenty four after the infusion, more than half of the attached cells in the decellularized liver scaffold (attached cells: 74 ± 13% of infused cells) were remained in the portal vein but they had moved into the parenchymal space at day 4 (Fig. 5b). The TUNEL-positive cells were gradually increased from 6.6 ± 2.7% at day 1 and 21 ± 8.6% at day 4 to 47.8 ± 5.4% at day 7 (Fig. 5c). Porcine livers (Fig. 5c) were decellularized (Fig. 5d) by the previously described method. Albumin staining after 4 and 7 days of culture-perfusion showed that hepatocytes engrafted around the larger vessels, repopulating the surrounding parenchymal area. The amount of immunostaining albumin of engrafted hepatocytes after 4 days of the perfusion culture was similar to that in normal livers; however, the expression decreased considerably after 7 days in the perfusion culture (Fig. 5e–i). The protein synthesis of infused cells was analyzed by the detection of albumin and urea concentration in the perfusion medium, compared to those in cultured porcine hepatocytes on collagen single layer. The albumin secretion (Fig. 5j) and urea synthesis level (Fig. 5k) was 8.7 ± 1.5 μg/1 × 10^6 cells/day and 181 ± 19 μg/1 × 10^6 cells/day at day 4, respectively, from perfusion-cultured hepatocytes in the scaffold and was 2.2 ± 0.6 μg/ml/1 × 10^6 cells and 137 ± 11.2 μg/ml/1 × 10^6 cells at day 4, respectively, from collagen-cultured hepatocytes. Although the protein synthesis was relatively higher in the perfusion-cultured hepatocytes, there was no significant difference in two groups for up to 7 days. However, when hepatocytes were cultured in a double-gel configuration (Fig. 5 j, k),

the albumin secretion was 22.9 ± 4.3 μg/ml/1 × 10^6 cells at day 4 and 16.9 ± 2.2 μg/ml/1 × 10^6 cells at day 7. Urea synthesis was 396 ± 13 μg/ml/1 × 10^6 cells at day 4 and 185 ± 18 μg/ml/1 × 10^6 cells at day 7. Double-gel cultured porcine hepatocytes demonstrated a superior albumin secretion and urea synthesis ability when compared with perfusion-cultured porcine hepatocytes or porcine hepatocytes cultured on collagen.

DISCUSSION

The present study describes a minimally disruptive method for whole-organ decellularization protocol in a large animal model that produces a three-dimensional liver matrix suitable for supporting functional hepatocytes, a broad characterization of the decellularized liver matrix shows maintenance of the hepatic matrix components and preservation of the vascular network, bile duct tree, and representative growth factors such as HGF, bFGF, VEGF, and IGF-1. Notably, we showed that reintroducing cells to the matrix is possible in large decellularized liver using a human-size organ culture system, resulting in approximately 74% grafting efficiency. The results of the present study not only confirm the concept of whole organ decellularization, as previously shown (5,19–21,24,27–29), but also provides methodology of organ engineering in a large size-scale adapted from previous rodent studies that will be important for clinical translation of this regenerative medicine approach for liver replacement.

To obtain a completely acellular porcine liver three-dimensional scaffold, we optimized a protocol that builds on the technique developed for heart perfusion decellularization by Ott et al. (20) and our own attempts in rat liver (29) demonstrating its applicability for large-scale liver decellularization. This decellularization protocol showed (i) preservation of the three-dimensional architecture, the native structural and basement membrane matrix, as well as the functional vascular network of the original organ including the biliary network; (ii) homogeneous and complete decellularization quantified by DNA content criterion in all the different segments of the liver; (iii) growth factor content can be preserved within the matrix scaffold at a level comparable to the native liver; and (iv) multistep cell seeding method showed high-efficiency engraftment of functional hepatocytes using a customized organ culture system. Moreover, Glisson's capsule was shown to be intact, an important feature because of anticipated future clinical applications in which hemorrhage after connection to an in vivo vascular supply would be problematic.

Whole-organ decellularization has been recently reported for different organs including liver (5,24,28,29); however, these whole-organ decellularization techniques have been scaled up to a clinically relevant size only for heart (30); moreover, most in vivo implantation in rodent studies has been limited to a few hours due to problems such as hemorrhage, thrombosis, and surgical technical difficulties. The method for whole-liver decellularization reported herein using porcine livers tackles and facilitates some of the issues (e.g., scalability, vascular integrity, external collagenous capsule integrity) that could determine ultimate clinical success.

Post decellularization process, the organs were translucent while preserving the three-dimensional architecture; moreover, immunostaining suggested that the matrix of both the large vessels (laminin) and the sinusoids (collagen type IV, fibronectin) remained intact. Furthermore, portal vein blood perfusion, corrosion casting, digital radiographic evaluation of the biliary tree, and SEM analysis demonstrate the presence and function of the microvascular network of the liver post decellularization.

The liver's ECM is a dynamic and functional structure that directly affects the fate and gene expression of liver cells (3,18). Moreover, growth factors and chemoattractants are

immobilized by ECM components through disulfide bonds (1). Thus, the precise ECM arrangement present in the adult liver could potentially facilitate and guide the developmental pathway for full hepatic maturation of stem cells. Thus, decellularized organs could potentially become a tool for stem cell differentiation and maturation to eventually engineer autologous liver grafts for transplantation (27). Liver cell sources to engineer liver grafts can primarily be obtained from livers rejected for orthotopic liver transplantation, unused segments of donor livers, and non-heart-beating donors. But, these sources do not begin to approach the potential numbers needed to treat all patients that might potentially benefit from auxiliary liver transplantation. Ideally, stem cells derived from the subject to be treated would be the perfect cell source to engineer personalized liver grafts. Induced pluripotent stem cells (iPS cells) have been created by transducing mature cells with transcription factors that transform them into cells that have characteristics and differentiation potential nearly identical to human embryonic stem cells (ES cells). While there is much enthusiasm for the potential use of stem cell-derived hepatocytes, generation of a sufficient mass of functional hepatocytes for treatment of liver failure from autologous cells derived from iPS cells would require a period of weeks for expansion, differentiation, selection, and testing to exclude contamination by tumorogenic precursors, far too long to address the problem of acute hepatic failure.

The importance of the determination of growth factors content in the decellularized livers is significant, and indeed this decellularization protocol can preserve approximately 19% of HGF, 20% of bFGF, 19% of VEGF, and 13% of IGF-1 content when compared to normal liver. These factors are essential in angiogenesis and hepatic regeneration and differentiation (8,12,25). In the present study, the decellularized native liver matrix was able to retain such growth factors after the whole decellularizing process, which may provide sufficient environmental cues to cells for survival and function. However, continuous production of angiogeneic factors (e.g., VEGF) would require the addition of endothelial cells.

Eventually rebuilding the entire sophisticated liver architecture will require addition of liver nonparenchymal cells, especially liver sinusoidal and microvascular endothelial cells to vascularize the entire graft and prevent thrombosis caused by direct exposure of the collagenous basement membrane to the circulation. In addition, biliary epithelial cells would be necessary in order to solve bile drainage. The multistep perfusion technique produced approximately 74% cell engraftment efficiency. The perfusion technique showed deposition of the primary hepatocytes within the parenchymal space and occasionally in the vessels. However, future studies will be performed in order to improve stability of hepatocicyte survival and function to achieve comparable function of double-gel culture hepatocytes (e.g., optimization of perfusion flow to decrease shear stress, hepatocyte cocultures, etc.).

Addition of nonparenchymal liver cells to reconstitute the sophisticated anatomy of the hepatic sinusoids are necessary, but the ultimate test is the transplantation in relevant animal models of liver failure;, thus, reliable models of liver failure in large animals will have to be developed.

In summary, the data presented herein provide a foundation for efficient development of clinically relevant liver scaffold and a cell-based regenerative medicine approach to build liver grafts for transplantation.

Acknowledgments

The authors thank Mr. Toshio Otake, Mr. Koji Matsumoto, and Ms. Keiko Kumagai from the Laboratory Animal Center; Dr. Ryo Nishiyama, Dr. Shunsuke Ichisaka, Dr. Yoshie Kadota, Dr. Haruto Sakamoto, Ms. Yumi Yoshimura, Ms. Reiko Nitta, and Ms. Katsuko Sano from Department of Surgery; Dr. Yasunori Okada from Department of Pathology; and Dr. Toshihiro Nagai from Electron Microscope Laboratory, School of Medicine,

Keio University. We would like to thank the Research Fellowship of the Japan Society for the Promotion of Science for young scientist to K.F. This study was supported by Keio University Special Grant-in-Aid for Innovative Collaborative Research Projects, a grant from Japan Society for the Promotion of Science KAKENHI (23689059), Takeda Science Foundation, the Mochida Memorial Foundation for Medical and Pharmaceutical Research, Kanae Foundation for the Promotion of Medical Science, and the Public Trust Fund for the Promotion of Surgery, Tokyo, Japan to H.Y. This work was also supported by a grant from NIH, DK083556 to A.S.-G.

References

1. Agrawal V, Johnson SA, Reing J, Zhang L, Tottey S, Wang G, Hirschi KK, Braunhut S, Gudas LJ, Badylak SF. Epimorphic regeneration approach to tissue replacement in adult mammals. Proc Natl Acad Sci USA. 2010; 107(8):3351–3355. [PubMed: 19966310]
2. Avolio AW, Frongillo F, Nicolotti N, Mule A, Vennarecci G, De Simone P, Agnes S. Successful use of extended criteria donor grafts with low to moderate steatosis in patients with model for end-stage liver disease scores below 27. Transplant Proc. 2009; 41(1):208–212. [PubMed: 19249515]
3. Badylak SF, Freytes DO, Gilbert TW. Extracellular matrix as a biological scaffold material: Structure and function. Acta Biomater. 2009; 5(1):1–13. [PubMed: 18938117]
4. Bao J, Shi Y, Sun H, Yin X, Yang R, Li L, Chen X, Bu H. Construction of a Portal implantable functional tissue engineered liver using perfusion-decellularized matrix and hepatocytes in rats. Cell Transplant. 2011; 20(5):753–766. [PubMed: 21054928]
5. Baptista PM, Siddiqui MM, Lozier G, Rodriguez SR, Atala A, Soker S. The use of whole organ decellularization for the generation of a vascularized liver organoid. Hepatology. 2011; 53(2):604–617. [PubMed: 21274881]
6. Crapo PM, Gilbert TW, Badylak SF. An overview of tissue and whole organ decellularization processes. Biomaterials. 2011; 32(12):3233–3243. [PubMed: 21296410]
7. Davis GL, Alter MJ, El-Serag H, Poynard T, Jennings LW. Aging of hepatitis C virus (HCV)-infected persons in the United States: A multiple cohort model of HCV prevalence and disease progression. Gastroenterology. 2010; 138(2):513–521. [PubMed: 19861128]
8. Desbois-Mouthon C, Wendum D, Cadoret A, Rey C, Leneuve P, Blaise A, Housset C, Tronche F, Le Bouc Y, Holzenberger M. Hepatocyte proliferation during liver regeneration is impaired in mice with liver-specific IGF-1R knockout. FASEB J. 2006; 20(6):773–775. [PubMed: 16484330]
9. Dunn JC, Yarmush ML, Koebe HG, Tompkins RG. Hepatocyte function and extracellular matrix geometry: Long-term culture in a sandwich configuration. FASEB J. 1989; 3(2):174–177. [PubMed: 2914628]
10. Gilbert TW, Freund JM, Badylak SF. Quantification of DNA in biologic scaffold materials. J Surg Res. 2009; 152(1):135–139. [PubMed: 18619621]
11. Hammond JS, Gilbert TW, Howard D, Zaitoun A, Michalopoulos G, Shakesheff KM, Beckingham IJ, Badylak SF. Scaffolds containing growth factors and extracellular matrix induce hepatocyte proliferation and cell migration in normal and regenerating rat liver. J Hepatol. 2011; 54(2):279–287. [PubMed: 21126791]
12. Kano MR, Morishita Y, Iwata C, Iwasaka S, Watabe T, Ouchi Y, Miyazono K, Miyazawa K. VEGF-A and FGF-2 synergistically promote neoangiogenesis through enhancement of endogenous PDGF-B-PDGFRbeta signaling. J Cell Sci. 2005; 118(Pt 16):3759–3768. [PubMed: 16105884]
13. Klein AS, Messersmith EE, Ratner LE, Kochik R, Baliga PK, Ojo AO. Organ donation and utilization in the United States, 1999–2008. Am J Transplant. 2010; 10(4 Pt 2): 973–986. [PubMed: 20420647]
14. Kollet O, Shivtiel S, Chen YQ, Suriawinata J, Thung SN, Dabeva MD, Kahn J, Spiegel A, Dar A, Samira S, Goichberg P, Kalinkovich A, Arenzana-Seisdedos F, Nagler A, Hardan I, Revel M, Shafritz DA, Lapidot T. HGF, SDF-1, and MMP-9 are involved in stress-induced human CD34+ stem cell recruitment to the liver. J Clin Invest. 2003; 112(2):160–169. [PubMed: 12865405]
15. Maruyama M, Totsugawa T, Kunieda T, Okitsu T, Shibata N, Takesue M, Kurabayashi Y, Oshita M, Nakaji S, Kodama M, Tanaka N, Kobayashi N. Hepatocyte isolation and transplantation in the pig. Cell Transplant. 2003; 12(6):593–598. [PubMed: 14579927]

16. Miki A, Rivas-Carrillo JD, Navarro-Alvarez N, Soto-Gutierrez A, Chen Y, Tanaka K, Narushima M, Tabata Y, Okitsu T, Noguchi H, Matsumoto S, Tanaka N, Kobayashi N. Maintenance of neovascularization at the implantation site of an artificial device by bFGF and endothelial cell transplant. Cell Transplant. 2006; 15(10):893–901. [PubMed: 17299994]
17. Moghe PV, Berthiaume F, Ezzell RM, Toner M, Tompkins RG, Yarmush ML. Culture matrix configuration and composition in the maintenance of hepatocyte polarity and function. Biomaterials. 1996; 17(3):373–385. [PubMed: 8745335]
18. Navarro-Alvarez N, Soto-Gutierrez A, Chen Y, Caballero-Corbalan J, Hassan W, Kobayashi S, Kondo Y, Iwamuro M, Yamamoto K, Kondo E, Tanaka N, Fox IJ, Kobayashi N. Intramuscular transplantation of engineered hepatic tissue constructs corrects acute and chronic liver failure in mice. J Hepatol. 2010; 52(2):211–219. [PubMed: 20022655]
19. Ott HC, Clippinger B, Conrad C, Schuetz C, Pomerantseva I, Ikonomou L, Kotton D, Vacanti JP. Regeneration and orthotopic transplantation of a bioartificial lung. Nat Med. 2010; 16(8):927–933. [PubMed: 20628374]
20. Ott HC, Matthiesen TS, Goh SK, Black LD, Kren SM, Netoff TI, Taylor DA. Perfusion-decellularized matrix: Using nature's platform to engineer a bioartificial heart. Nat Med. 2008; 14(2):213–221. [PubMed: 18193059]
21. Petersen TH, Calle EA, Zhao L, Lee EJ, Gui L, Raredon MB, Gavrilov K, Yi T, Zhuang ZW, Breuer C, Herzog E, Niklason LE. Tissue-engineered lungs for in vivo implantation. Science. 2010; 329(5991):538–541. [PubMed: 20576850]
22. Schneider MK, Seebach JD. Xenotransplantation literature update, July–October 2011. Xenotransplantation. 2011; 18(6):400–404. [PubMed: 22168146]
23. Sellaro TL, Ranade A, Faulk DM, McCabe GP, Dorko K, Badylak SF, Strom SC. Maintenance of human hepatocyte function in vitro by liver-derived extra-cellular matrix gels. Tissue Eng Part A. 2010; 16(3):1075–1082. [PubMed: 19845461]
24. Shupe T, Williams M, Brown A, Willenberg B, Petersen BE. Method for the decellularization of intact rat liver. Organogenesis. 2010; 6(2):134–136. [PubMed: 20885860]
25. Soto-Gutierrez A, Kobayashi N, Rivas-Carrillo JD, Navarro-Alvarez N, Zhao D, Okitsu T, Noguchi H, Basma H, Tabata Y, Chen Y, Tanaka K, Narushima M, Miki A, Ueda T, Jun HS, Yoon JW, Lebkowski J, Tanaka N, Fox IJ. Reversal of mouse hepatic failure using an implanted liver-assist device containing ES cell-derived hepatocytes. Nat Biotechnol. 2006; 24(11):1412–1419. [PubMed: 17086173]
26. Soto-Gutierrez A, Navarro-Alvarez N, Yagi H, Nahmias Y, Yarmush ML, Kobayashi N. Engineering of an hepatic organoid to develop liver assist devices. Cell Transplant. 2010; 19(6): 815–822. [PubMed: 20573303]
27. Soto-Gutierrez A, Yagi H, Uygun BE, Navarro-Alvarez N, Uygun K, Kobayashi N, Yang YG, Yarmush ML. Cell delivery: From cell transplantation to organ engineering. Cell Transplant. 2010; 19(6):655–665. [PubMed: 20525441]
28. Soto-Gutierrez A, Zhang L, Medberry C, Fukumitsu K, Faulk D, Jiang H, Reing J, Gramignoli R, Komori J, Ross M, Nagaya M, Lagasse E, Stolz D, Strom SC, Fox IJ, Badylak SF. A whole-organ regenerative medicine approach for liver replacement. Tissue Eng Part C Methods. 2011; 17(6): 677–686. [PubMed: 21375407]
29. Uygun BE, Soto-Gutierrez A, Yagi H, Izamis ML, Guzzardi MA, Shulman C, Milwid J, Kobayashi N, Tilles A, Berthiaume F, Hertl M, Nahmias Y, Yarmush ML, Uygun K. Organ reengineering through development of a transplantable recellularized liver graft using decellularized liver matrix. Nat Med. 2010; 16(7):814–820. [PubMed: 20543851]
30. Wainwright JM, Czajka CA, Patel UB, Freytes DO, Tobita K, Gilbert TW, Badylak SF. Preparation of cardiac extracellular matrix from an intact porcine heart. Tissue Eng Part C Methods. 2010; 16(3):525–532. [PubMed: 19702513]
31. Yamanouchi K, Zhou H, Roy-Chowdhury N, Macaluso F, Liu L, Yamamoto T, Yannam GR, Enke C, Solberg TD, Adelson AB, Platt JL, Fox IJ, Roy-Chowdhury J, Guha C. Hepatic irradiation augments engraftment of donor cells following hepatocyte transplantation. Hepatology. 2009; 49(1):258–267. [PubMed: 19003915]

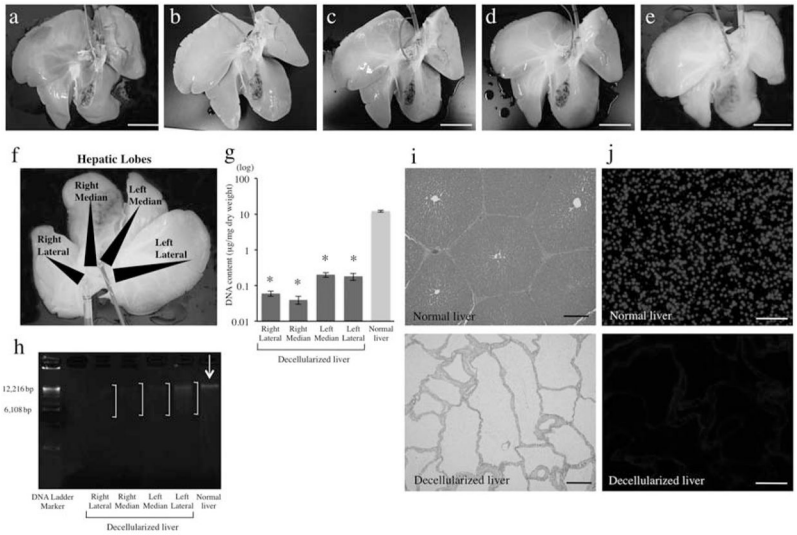

Figure 1.

Whole-organ porcine liver homogeneous decellularization. Representative images of porcine livers during decellularization process at (a) 0 h, (b) 18 h, (c) 48 h, (d) 72 h, and (e) 96 h. (f) DNA was extracted from each different lobe. (g) The DNA content of different lobes of the decellularized liver matrix ($n = 4$ for each lobe) and (h) agarose gel electrophoresis of extracted DNA comparing to that of normal porcine liver. Histological comparison of normal liver and decellularized liver matrix: (i) hematoxylin and eosin. (j) The presence of intact nuclear material was evaluated by staining the decellularized liver and native liver using 4′,6-diamidino-2-phenylindole (DAPI). *$p < 0.01$. Scale bars: 5 cm (a–e) and 100 μm (h, i).

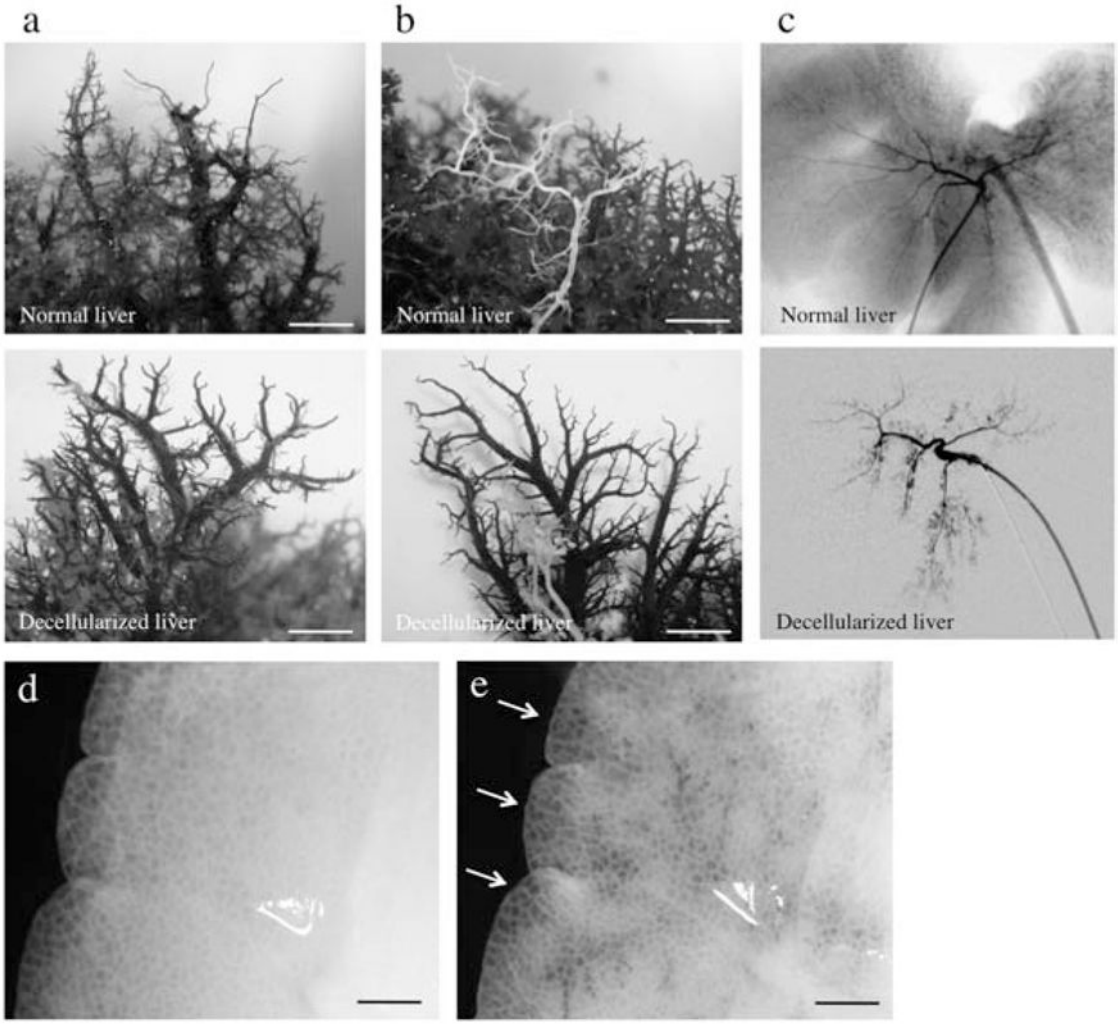

Figure 2.

Decellularized liver matrix preserves entire vascular system and bile ducts. Representative photographs of decellularized left lobes of porcine liver, with the vascular tree visible. Comparison of normal liver and decellurarized whole-liver bioscaffold of corrosion cast of (a) portal vein (lighter staining) and hepatic artery (darker staining) and (b) hepatic vein and bile duct (white) as well as by (c) radiographic imaging of the bile ducts. (d, e) Representative photographs of visible microvascular tree, after perfusion with heparinized porcine blood through the portal vein. Scale bars: 100 μm.

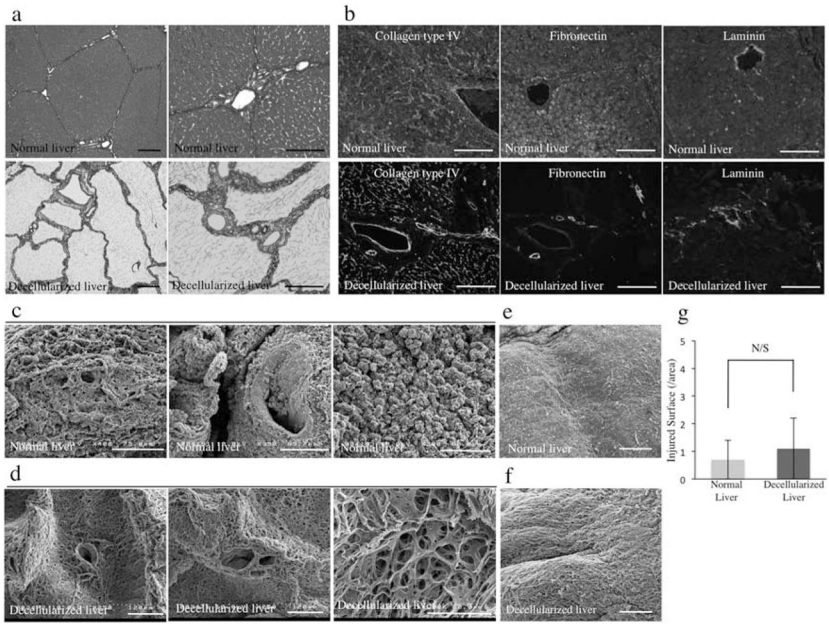

Figure 3.

Morphology. (a) Azan stain of normal porcine livers and decellularized porcine liver scaffolds. (b) Immune-histochemical stain of normal porcine livers (top row) and decellularized porcine liver scaffolds (bottom row) of collagen IV, fibronectin, and laminin. Sections were counterstained with DAPI. (c) SEM images of normal porcine liver and (d) decellularized porcine liver scaffold; representing central vein, portal triad, and extracellular matrix within the parenchyma. (e) Representative photographs of normal and (f) decellularized porcine liver surface (Glisson's capsule) and (g) the quantification of disruptive areas in the collagenous surface of the livers ($n = 4$: 10 random images for each sample). Scale bars: 100 and 50 μm (third picture of (c) and (d)). N/S, no significant difference.

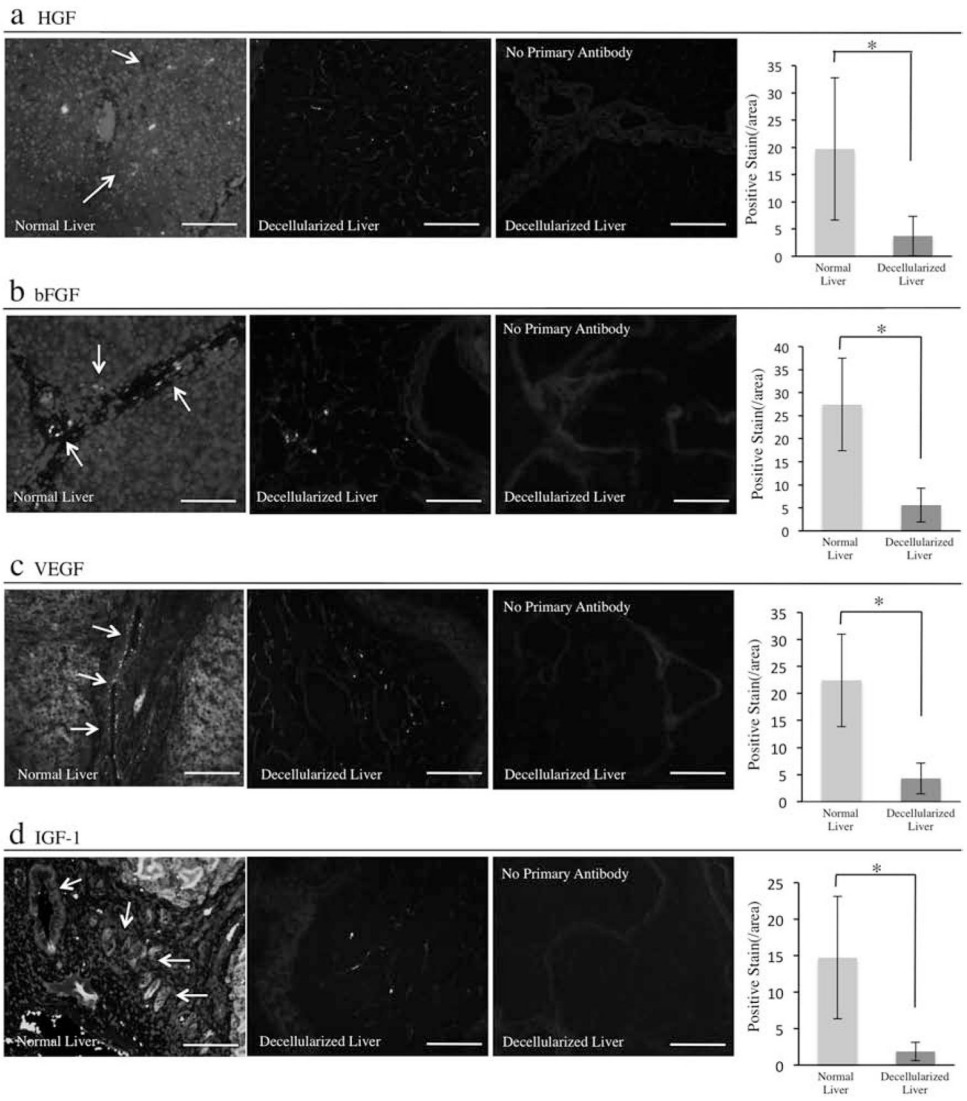

Figure 4.

Decellularized whole-liver scaffold retained growth factors expression. Immune-histochemical evaluation of growth factors. (a) Hepatocyte growth factor (HGF) stain of native liver and the acellular liver scaffold and its quantification of the positive areas (arrows) per field ($n = 4$: 10 random images for each sample). (b) Basic fibroblast growth factor (bFGF) stain of native liver and the acellular liver scaffold and its quantification of the positive areas (arrows) per field ($n = 4$: 10 random images for each sample). (c) Vascular endothelial growth factor (VEGF) stain of native liver and the acellular liver scaffold and its quantification of the positive areas (arrows) per field ($n = 4$: 10 random images for each sample). (d) Insulin-like growth factor (IGF)-1 stain of native liver and the acellular liver scaffold and its quantification of the positive areas (arrows) per field ($n = 4$: 10 random images for each sample). Immunostain without primary antibodies with secondary antibodies served as controls in each experiment. Scale bars: 100 μm. *$p < 0.05$.

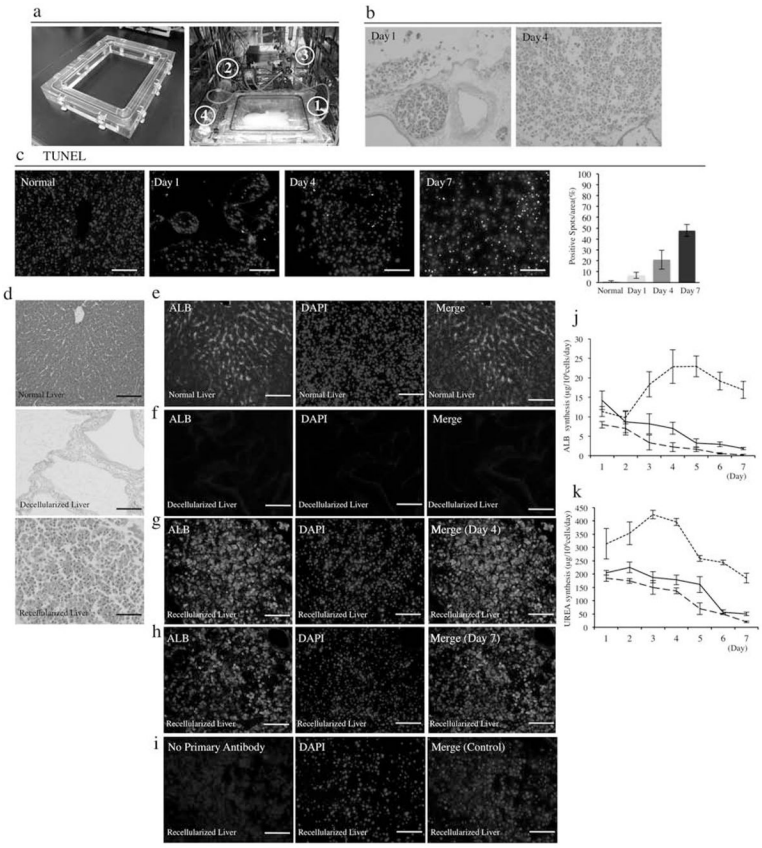

Figure 5.

Recellularization of a large-scale liver scaffold using porcine primary hepatocytes. (a) Representative photograph of the chamber constructed specifically for a large-scale liver graft and the liver perfusion system (1: closed chamber, 2: peristaltic pump, 3: bubble trap, 4: oxygenator). (b) H&E stain of infused cells in the decellularized liver at day 4 and day 7 (n = 4). (c) Sequential images of terminal deoxynucleotidyl transferase dUTP nick end labeling (TUNEL) stain at different time points and quantitative analysis of TUNEL positive cells (n = 4: 10 random images for each sample). (d) Histological images of normal liver, decellularized liver scaffold, and recellularized liver with primary porcine hepatocytes for H&E stain (n = 4). (e) Albumin (ALB) stain of normal porcine liver, (f) decellularized liver, and recellularized liver with primary porcine hepatocytes after 4 days (g) and 7 days (h) of perfusion. (i) Immunostain without the primary antibody with secondary antibody served as control (n = 4). (j) ALB concentration in the culture medium of collagen-Matrigel sandwich culture (small dashes) or single collagen culture of normal porcine hepatocytes (large dashes) and in the perfusion culture medium of recellularized liver (n = 3). (k) UREA concentration in the culture medium of collagen-Matrigel sandwich culture (small dashes) or single collagen culture of normal porcine hepatocytes (large dashes) and in the perfusion culture medium of recellularized liver (black line) (n = 3). Sections were counterstained with DAPI. Scale bars: 100 μm.